Available online at www.sciencedirect.com
SCIENCE DIRECT®
Journal of Nuclear Materials 350 (2006) 320–331
journal of nuclear materials
www.elsevier.com/locate/jnucmat

The influence of calcium ions on the development of acidity in corrosion product deposits on SIMFUEL, UO_2

B.G. Santos *, J.J. Noël, D.W. Shoesmith

Department of Chemistry, The University of Western Ontario, 1151 Richmond Street, London, Ont., Canada N6A 5B7

Received 20 October 2005; accepted 1 February 2006

Abstract

In order to clarify the influence of groundwater constituents on the formation of corrosion products and secondary phase deposits on corroding/dissolving nuclear fuel surfaces under waste disposal conditions we have investigated the influence of Ca^{2+}, present as $CaCl_2$. The influence of calcium ions on the anodic dissolution of SIMFUEL (doped uranium dioxide) has been characterized over the potential range 0–500 mV (vs. SCE). Through the use of X-ray photoelectron spectroscopy (XPS) the surface composition over this potential range has been determined. Ca^{2+} was found not to influence the conversion of $U^{IV}O_2$ to $U^{IV}_{1-2x}U^{V}_{2x}O_{2+x}$, but to suppress the subsequent formation of a U^{VI} surface species which lead to the formation of a hydrated deposit, $UO_3 \cdot yH_2O$. The adsorption of Ca^{2+} on the UO_2 surface is believed to inhibit fuel dissolution either via inhibiting the stabilization of the cation precursor $(UO_2(OH)_2)_{ads}$ or by blocking the O^{2-} anion transfer reaction from the fuel surface.

1. Introduction

Over the past 25 years or more a substantial effort has been expended to study fuel dissolution and radionuclide release processes under a range of proposed waste repository conditions [1]. Under granitic conditions (i.e., in the repositories proposed in Canada, Sweden, and Finland), anoxic conditions will be rapidly established since environmental oxidants such as dissolved O_2, trapped in the repository on sealing, will be quickly scavenged by reaction with the Cu container material, oxidizable minerals, or organic material present in the repository environment [2]. Since the container is expected to long outlive the oxic period, anoxic conditions should prevail at the time of container penetration. Thus, the primary source of oxidants to drive fuel corrosion, and hence radionuclide release, will be the radiolysis of water, due to the radiation fields emanating from the spent fuel.

It is reasonable to assume that waste containers will survive the period when β/γ fields are significant (300–1000 years [3]) and hence, that only the α-radiolysis of water will be a significant source of oxidants [4]. Since α-radiation fields will decay with time, the redox conditions at the surface of the fuel will change with time, and, over the repository lifetime the composition of the fuel surface should, therefore,

* Corresponding author.
E-mail address: bsantos@uwo.ca (B.G. Santos).

0022-3115/$ - see front matter © 2006 Published by Elsevier B.V.
doi:10.1016/j.jnucmat.2006.02.002

evolve. This evolution will involve the accumulation of corrosion/dissolution product deposits on the surface of the fuel. The accumulation of deposits will have a number of distinct effects:

(i) It could block the fuel surface, thereby reducing the available exposed surface area and suppressing the rate of fuel corrosion.
(ii) It could restrict the diffusive mass transport of species to (e.g., Fe^{2+}, H_2) and from (e.g., H_2O_2, $UO_2(OH)_y^{(2-y)+}$) the reacting surface. This could lead to localized chemistries within pores in the deposits such as the accumulation of radiolytically-produced H_2O_2 and/or the development of localized acidity due to the hydrolysis of dissolved uranium [5].
(iii) It could co-precipitate α-emitting radionuclides, such as ^{237}Np, thereby modifying the yield and distribution of α-radiolysis products [6–9].

The physical and chemical properties of deposits formed on fuel surfaces will be determined primarily by the combination of redox conditions, temperature and groundwater composition. An accumulation of evidence exists to show corrosion product deposits form under both moist vapour and fully immersed conditions. Buck et al. [7] characterized the nature of the deposits formed in aerated vapour at 90 °C on spent fuel. Not surprisingly, a relatively simple combination of uranyl oxy-hydroxide alteration phases, dehydrated schoepite ($(UO_2)O_{0.25-x}(OH)_{1.5+2x}$ ($0 \leqslant x \leqslant 0.15$)) and metashoepite, is formed [10] and after 924 days of exposure, the thickness of the deposit was 100–200 μm. The influence of groundwater species has been investigated in detail in drip tests with UO_2 at 90 °C [11–13]. These experiments used high (0.075 mL/3.5 days) and low (0.0375 mL/7 days) drip rates of equilibrated J-13 water, a Na^+, Ca^{2+} and silicate containing water anticipated within Yucca Mountain [14]. In both sets of tests Na^+, Ca^{2+} and silicate were incorporated into the U^{VI} oxides/hydroxides formed. In low drip rate tests dehydrated schoepite, soddyite ($(UO_2)_2SiO_4 \cdot 2H_2O$), and possibly sodium compreignacite ($Na_2[(UO_2)_6(OH)_6] \cdot 8H_2O$), were formed. At high drip rates, when the supply of Na^+, Ca^{2+} and silicate is more copious, the uranophane-group silicates, β-uranophane ($Ca(UO_2)_2(SiO_3OH)_2(H_2O)_5$) and sodium boltwoodite ($(Na,K)(UO_2)(SiO_3OH)(H_2O)$), were formed [11]. The approximately constant rate of release of dissolved uranium over the >8 years of testing shows that the development and transformation of phases did not lead to any observable suppression of the fuel corrosion rate. This inability to suppress corrosion is probably a consequence of the convective influence of the drips, since under fully immersed conditions; the transition from a uranyl phase deposit to a more compact mineral silicate layer was thought to occur over a period of several weeks [15]. Since, in these last experiments [15], the rates of U release were not measured, the protectiveness of this layer is not readily assessed.

Similarities in the alteration phases observed in laboratory experiments to those observed in the geological alteration of natural uraninite deposits provides evidence that the overall alteration processes observed in the laboratory are similar to those likely to control alteration in the long term [11,16,17]. Studies of uranium deposits exposed to oxidizing conditions clearly demonstrate the incorporation of Ca^{2+} and silicate into oxidized uranium phases such as becquerelite, soddyite, weeksite, boltwoodite and β-uranophane [14]. U^{VI} silicates, such as uranophane, are believed to be among the thermodynamically stable phases that will form following the alteration of spent nuclear fuel in the Yucca Mountain repository on a geologic timescale [18].

Amme et al. [19] investigated potential alteration mechanisms for UO_2 in contact with the groundwater ions, Ca^{2+}, CO_3^{2-} and silicate, under the anoxic conditions expected to prevail eventually in granitic repositories. Of these, only dissolved Si had a measurable effect, producing a significant decrease in the concentration of dissolved U. Attempts to analyze alteration products on the surface of the fuel were only partially successful, despite conducting experiments at 180 °C. SEM/EDX analyses found deposits with a U:Si ratio of 1:1, as expected for coffinite ($USiO_4 \cdot nH_2O$) but XRD analyses failed to confirm its presence. Minor amounts of a second phase with elemental ratios close to those expected for ekanite ($U(Ca,Fe)_2Si_8O_{20}$) were also observed.

A special feature of corrosion in the presence of water radiolysis (or added H_2O_2, the radiolytic oxidant of primary interest) is the possibility of forming uranium peroxide secondary phases, particularly studtite ($UO_4 \cdot 4H_2O$). This phase has been found in nature [20], observed in mineral leaching experiments [21,22], spent fuel leaching experiments along with metastudtite ($UO_4 \cdot 2H_2O$) [23], UO_2 dissolution experiments [24–26] and in UO_2 dissolution experiments in the presence of ^4He radiation [27].

The properties of studtite have been described [28,29]. Since these phases are unstable in the absence of H_2O_2 they would be expected only as transitory phases when α-radiation fields are substantial, and are unlikely to exert a significant influence on fuel corrosion/dissolution rates in the long term, when such radiation fields are too weak to produce meaningful concentrations of peroxide.

The chart in Fig. 1 summarizes the phases anticipated under different redox conditions based on these studies. The mineralogy of U is extremely complex [18], and the phases given represent general observations and not an exhaustive list of possibilities. The mixed U^{IV}/U^{VI} solid, ianthinite ($U^{IV}(U^{VI}O_2)_5(OH)_{14}\cdot 3H_2O$), has been observed under oxidizing conditions [30], but the authors speculated that its formation was a consequence of local depletions of oxidants at the sites at which it was formed.

A review of the chart shows a complicated range of phases could be formed as redox conditions evolve from initially oxidizing to eventually anoxic. A primary feature of these phases is the general incorporation of Na^+, Ca^{2+} and the formation of silicates, indicating that these groundwater constituents could exert a major influence on fuel corrosion over extended periods of time. However, the species Ca^{2+} and SiO_4^{4-} have been shown to directly influence the corrosion rate of UO_2 in single-pass flow-through experiments when the formation of deposits on the fuel surface would not be expected.

Uranium concentrations measured in single-pass flow-through experiments with unirradiated UO_2 pellet fragments showed that the effect of adding $15\ mg\ L^{-1}$ of Ca^{2+} to a $2\times 10^{-3}\ mol\ L^{-1}$ HCO_3^- solution decreased the concentration of U in the effluent solution by a factor of 3 [31]. A subsequent addition of $30\ mg\ L^{-1}$ of SiO_4^{4-} increased this suppression by a further factor of 100. Auger analysis of the UO_2 surface indicated a thin layer containing Ca and Si was present on the surface, despite the use of a flow-through system to prevent deposition. Tait and Luht [32], observed a similar suppression of the UO_2 corrosion rate by a factor of 200, using a similar experimental system. They also showed that the corrosion rate of spent fuel and the release of radionuclides were suppressed by a similar factor in a groundwater containing Ca^{2+} and SiO_4^{4-}.

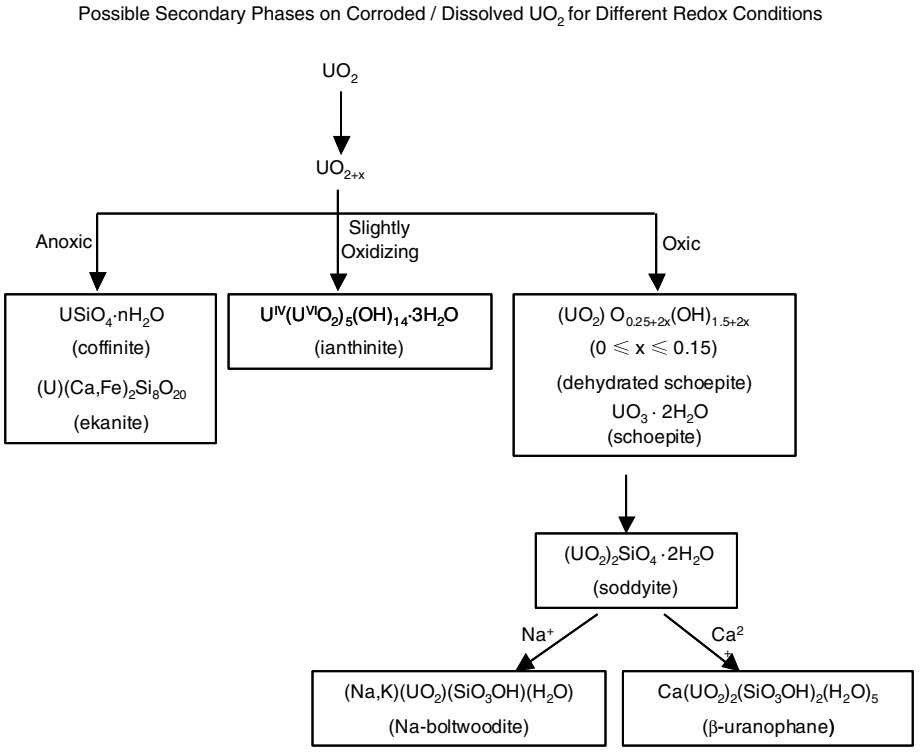

Fig. 1. Schematic showing the possible secondary phases that could form on corroded/dissolved UO_2 surfaces for different redox conditions.

The fact that the corrosion rate response to the addition of Ca/Si is so fast suggests that, if the ions are incorporated into U^{VI} phases with very low solubilities, very little of these phases is required to suppress corrosion. Alternatively, adsorption of Ca/Si on the fuel surface could suppress the anodic fuel step directly. Both of these possibilities are consistent with electrochemical experiments [33].

To date, our electrochemical studies have been limited to $NaClO_4$ and NaCl solutions [4,33,40,46]. These studies have elucidated the change in composition of the UO_2 surface as a function of redox conditions including the conditions when U^{VI} species begin to accumulate on the corroding surface. As part of a larger project to clarify the influence of groundwater constituents on the formation of corrosion product and secondary phase deposits, we have studied the influence of Ca^{2+} and Si on film corrosion. Here, we present the results of our studies on the influence of Ca^{2+}, present as $CaCl_2$.

2. Experimental

2.1. Fuel specimens

The electrodes used in this study were 1.5 at.% SIMFUEL made from pellets fabricated at Chalk River Laboratories, Ontario. These are natural UO_2 pellets doped with non-radioactive elements (Ba, Ce, La, Mo, Sr, Y, Zr, Rh, Pd, Ru, and Nd) to replicate the chemical effects of a CANDU reactor irradiation to 1.5 at.% burn up [34]. The trivalent rare earth elements (RE^{3+}) act as dopants in the U^{IV} oxide lattice and increase the number density of donor–acceptor sites in the fuel, leading to an increase in electronic conductivity [34–36]. The noble, and other, metal dopants (Pd, Ru, Mo, Rh) are stabilized in the fuel lattice as metallic particles, known as ε-particles. Simulated fuels of this type provide a practical means to study the effect on fuel corrosion of the impurities created by in-reactor fission [37–39]. The electrode resistance measured by electrochemical impedance spectroscopy (EIS) was 55 Ω [40].

2.2. Electrode preparation

The SIMFUEL electrodes were prepared using a methodology previously described [40]. Prior to use, the electrode was polished (wet) with a 600 grit SiC paper, rinsed with distilled deionized water and repolished (wet) with 1200 grit SiC paper.

2.3. Solutions

The solutions used were various combinations of NaCl and $CaCl_2$ at a concentration of 0.1 mol L^{-1} adjusted to pH = 9.5. All solutions were prepared with distilled deionized water purified using a Millipore milli-Q-plus unit to remove organic and inorganic impurities. All chemicals were reagent grade and purchased from Fisher Scientific. Solution pH was monitored with an Orion model 720A pH meter. The pH was adjusted with reagent grade HCl or NaOH. Since we observed no influence of chloride ions on the fuel dissolution process it was deemed unnecessary to control solution ionic strength.

2.4. Electrochemical cell and equipment

All experiments were conducted in a three-electrode, three compartment cell. The central chamber of the cell was separated from the reference and counter electrode chambers by glass frits. The counter electrode was made of Pt foil spot welded to a Pt wire. All potentials were measured, and are quoted, against a saturated calomel reference electrode (SCE). All electrochemical experiments were performed with a Solartron 1287 potentiostat controlled by Corrware software.

2.5. Surface analysis

X-ray photoelectron spectroscopy (XPS) was used to characterize the surface films formed electrochemically. An SSX-100 spectrometer was used to record the XPS spectra. The U ($4f_{7/2}$), satellites associated with U ($4f_{5/2}$) and the valence band regions of the UO_2 spectrum were recorded. The procedure used to analyze these regions involved a fitting routine which was 70% Gaussian and 30% Lorentzian with a Shirley background correction [41]. The XPS band at ~380 eV, resulting from the ejected $4f_{7/2}$ electrons, was used to monitor the chemical state of uranium atoms. The proportions of uranium oxidation states U^{IV}, U^{V} and U^{VI} in the electrode surface were determined by fitting the $4f_{7/2}$ peak using accepted binding energies (U^{IV} −379.9 eV, U^{V} −380.4 eV and U^{VI} −381.3 eV) and spectral satellite analyses as previously described [40,42]. The position of the C (1*s*) line at 284.6 eV was recorded and used, when necessary,

to correct for surface charging. The peak position used for Ca ($2p_{3/2}$) was 247 eV [43].

Scanning electron microscopy (SEM) was used for high-resolution imaging of surfaces. A Hitachi S-4500 field emission SEM was used in this study.

3. Results

3.1. Voltammetric behaviour

Fig. 2 shows two voltammograms illustrating the stages of oxidation and reduction recorded at a scan rate of 10 mV/s on SIMFUEL at pH = 9.5 in 0.1 mol L^{-1} NaCl and 0.1 mol L^{-1} $CaCl_2$, respectively. Oxidation of the surface commences around ~ -300 mV and the shallow current in region [I] has been shown to be due to the oxidation of stoichiometric UO_2 grains to UO_{2+x} up to a limiting composition of $UO_{2.33}$ [1,44]. The increasing current in region [II] ($\geqslant 200$ mV) is attributed to the further oxidation of this UO_{2+x} layer to soluble UO_2^{2+} species. At a pH of 9.5, UO_2^{2+} possesses a limited solubility [45], and precipitates on the electrode surface. Comparison of the two scans suggests that Ca^{2+} has no significant influence on oxidation of the surface to UO_{2+x} [I] but may suppress dissolution as UO_2^{2+} [II]. On the reverse scan, reduction of the anodically formed $UO_{2+x}/UO_3 \cdot yH_2O$ layer is observed in region [III]. Reduction peak [III] is smaller in Ca^{2+} consistent with a suppression of dissolution, and hence the deposition of $UO_3 \cdot yH_2O$ (region II), compared to Na^+-dominated solutions.

3.2. Constant potential current–time behaviour (1 h)

Fig. 3 shows potentiostatic current–time curves recorded for 1 h at potentials in the range 100–500 mV in 0.1 mol L^{-1} $CaCl_2$. A large majority of this current produces soluble species which may, or may not, be subsequently deposited on the electrode surface. Consequently, it can be considered a dissolution current. The general features of the current responses are similar to those observed previously [40] in NaCl, though not as consistent. At lower applied potentials, the current decreases logarithmically with time, consistent with previous observations at pH = 9.5, due to the growth of a thin UO_{2+x} surface layer. The location of the shoulder (previously attributed to the onset of formation of a U^{VI} surface layer [40]) is not as consistent with applied potential as observed under similar conditions in NaCl.

Fig. 4 shows a direct comparison of oxidation at 200 mV ((i)–(ii)) and 500 mV ((iii)–(iv)) over a 1 h period in a Ca^{2+}-dominated vs. a Na^+-dominated solution. At 200 mV, the current at longer times is consistently lower in Ca^{2+} solution ((i) compared to (ii) in Fig. 4) indicating a suppression of the overall $UO_2 \rightarrow UO_{2+x}/UO_3 \cdot yH_2O$ oxidation/dissolution/deposition process. At 500 mV, Fig. 4 ((iii) and (iv)), a similar suppression is apparent at short times but, at longer times, the current in Ca^{2+} solution (iii) recovers to the value observed in Na^+ solution (iv). The achievement of a steady-state, and sometimes increased, current at long times at such a positive potential has been shown to be due to

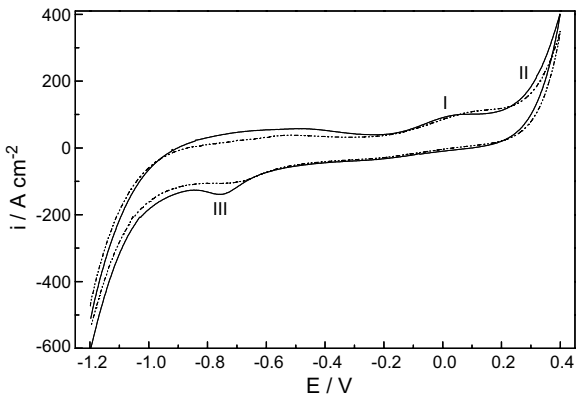

Fig. 2. Voltammograms recorded at a scan rate of 10 mV s^{-1} in 0.1 mol L^{-1} NaCl (—) and 0.1 mol L^{-1} $CaCl_2$ (---·---) to an anodic potential limit of 0.4 V at pH 9.5. Regions I, II and III are discussed in the text.

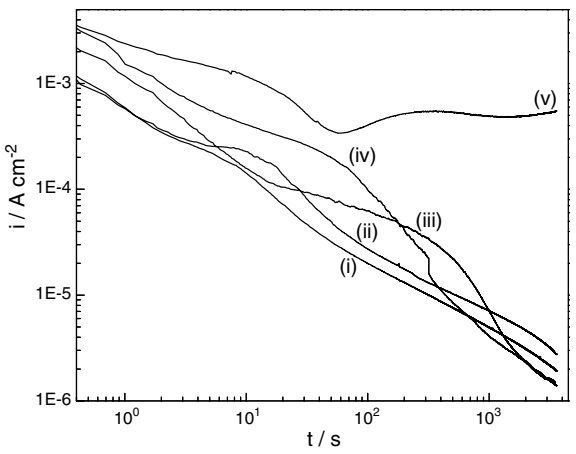

Fig. 3. Potentiostatic current–time curves recorded for 1 h in 0.1 mol L^{-1} $CaCl_2$ at potentials of (i) 100 mV, (ii) 200 mV, (iii) 300 mV, (iv) 400 mV and (v) 500 mV at pH 9.5.

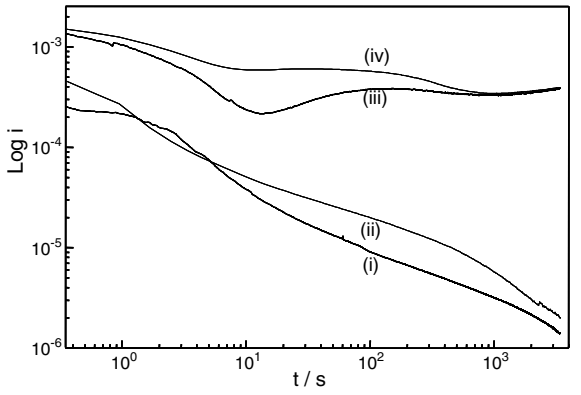

Fig. 4. Potentiostatic current–time curves recorded for 1 h in 0.1 mol L^{-1} $CaCl_2$ [(i) and (iii)] and 0.1 mol L^{-1} NaCl [(ii) and (iv)] at potentials of 200 mV [(i)–(ii)] and 500 mV [(iii)–(iv)] at pH 9.5.

the development of acidity within local sites on the rough fuel surface due to rapid dissolution and hydrolysis [40,46]. While the lower short-term suppression of the current at 500 mV suggests this development of acidity may be initially suppressed by Ca^{2+}, thereby suppressing the dissolution current, it cannot be prevented.

3.3. X-ray photoelectron spectroscopy after oxidation (1 h)

Fig. 5 shows an XPS survey spectrum taken after anodically oxidizing the UO_2 surface at 100 mV for 1 h. As expected [43], a Ca ($2p_{3/2}$) peak is found at 347 eV. Since a signal for Cl^- is also observed in the survey spectra it is possible that the presence of Ca^{2+} is due to the precipitation of the $CaCl_2$ electrolyte on extracting the electrode from the cell, since the washing procedure could be partially ineffective if $CaCl_2$ was trapped in asperities on the rough electrode surface. While the amount of Ca^{2+} on/in the electrode surface varies from 3.50% (300 mV) to 5.25% (500 mV) it does not vary systematically with potential or the percentage of Cl^- present in/on the surface. Thus, there is no consistent evidence in these data for incorporation of Ca^{2+} into the electrode surface by any mechanism other than electrolyte precipitation.

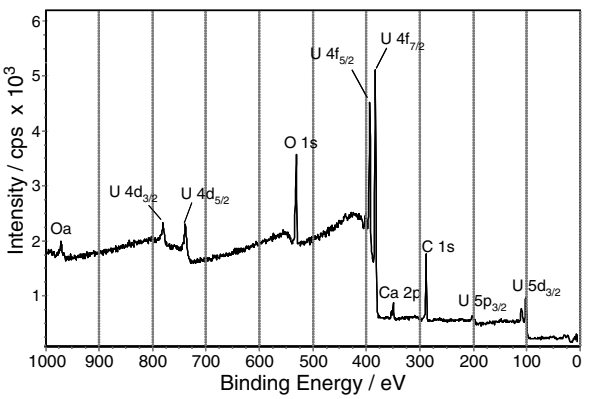

Fig. 5. XPS survey spectrum recorded on a UO_2 surface after 1 h in 0.1 mol L^{-1} $CaCl_2$ at 100 mV.

Fig. 6(A) and (B) show a comparison between the U($4f_{7/2}$) peak resolved into contributions from the three possible oxidation states of U after 1 h oxidation at 100 mV in 0.1 mol L^{-1} $CaCl_2$ and 0.1 mol L^{-1} NaCl, respectively. These deconvolutions reveal that the amount of U^{VI} on the UO_2 surface is suppressed in $CaCl_2$ (8% U^{VI}) compared to NaCl (28% U^{VI}), thereby maintaining a generally U^{IV}/U^{V} dominated surface. The higher U^{V} and lower U^{VI}, contents of the surface suggest that Ca^{2+} does not influence the surface oxidation process

$$UO_2 + xH_2O \rightarrow U^{IV}_{1-2x}U^{V}_{2x}O_{2+x} + 2xH^+ + 2xe^- \quad (1)$$

but suppresses the subsequent formation of surface U^{VI} species which are thought to form via a dissolution (as UO_2^{2+})–deposition ($UO_3 \cdot yH_2O$) process. These observations are consistent with the lower currents observed in voltammetric (Fig. 2, region 2) and potentiostatic (Fig. 3) experiments.

Fig. 7 shows the proportions of the three oxidation states as a function of applied potential after 1 h in 0.1 mol L^{-1} $CaCl_2$ for the entire potential range investigated. Though the behaviour observed in $CaCl_2$ is generally similar to that obtained in NaCl [37] over the same potential range, a number of points are emphasized:

(i) The high U^{V} content at 100 mV indicates the presence of the $U^{IV}U^{V}O_{2+x}$ layer in the presence of Ca^{2+}. The dominance of this layer is consistent with the form of the $\log I$–$\log t$ plot (Fig. 3) which shows an approximately linear decrease.

(ii) The increasing dominance of U^{VI} with increasing potential is consistent with the development of a shoulder in the $\log I$–$\log t$ plot attributed to the accumulation of U^{VI} on the UO_{2+x} surface.

(iii) The drop in U^{VI} and increase in U^{IV} at the highest applied potential, 500 mV, indicates the re-dissolution of U^{VI} and exposure of the underlying $U^{IV}U^{V}O_{2+x}$ surface due to local acidification.

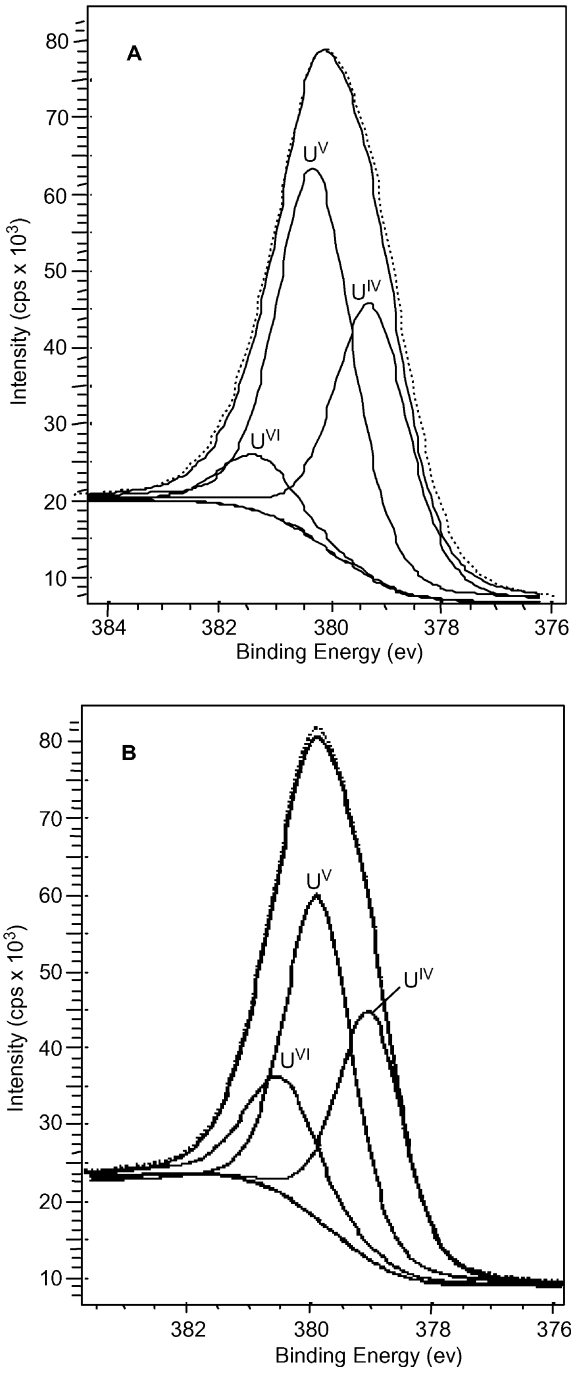

Fig. 6. Deconvolution of the U $4f_{7/2}$ XPS peak into three contributions (U^{IV}, U^V and U^{VI}) on an electrode anodically oxidized at 100 mV for 1 h in (A) 0.1 mol L^{-1} $CaCl_2$ and (B) 0.1 mol L^{-1} NaCl (pH 9.5).

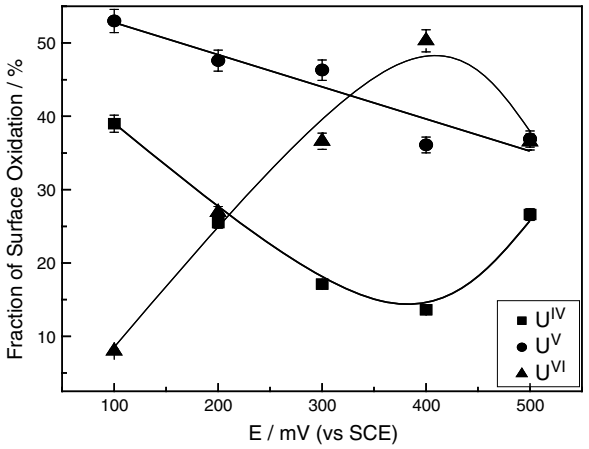

Fig. 7. Relative fractions of all three U oxidation states as a function of applied potential after anodic oxidation in 0.1 mol L^{-1} $CaCl_2$.

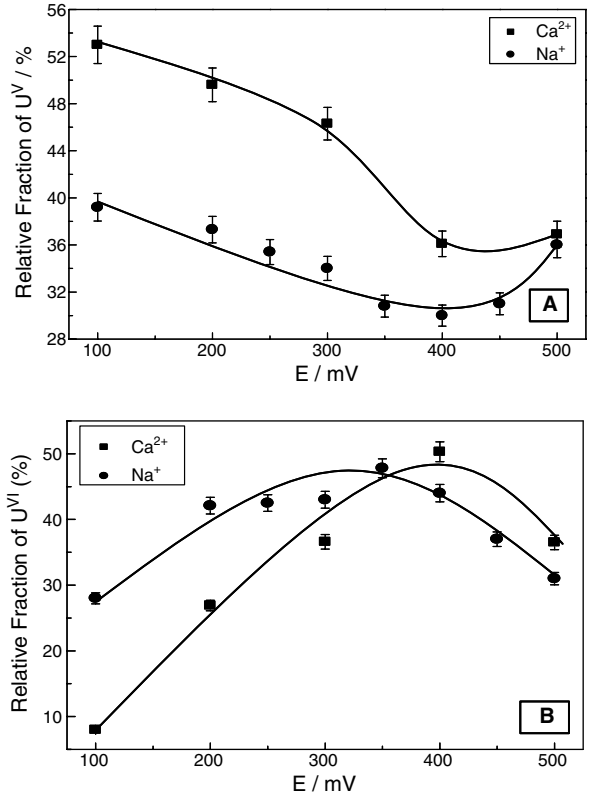

Fig. 8. A comparison of the relative fractions of (A) U^V and (B) U^{VI} as a function of applied potential in 0.1 mol L^{-1} $CaCl_2$ and 0.1 mol L^{-1} NaCl (pH 9.5).

Fig. 8 compares the relative fractions of U^V and U^{VI} on the UO_2 surface in 0.1 mol L^{-1} NaCl and 0.1 mol L^{-1} $CaCl_2$. The results confirm that the electrochemical oxidation of the electrode surface from U^V to U^{VI} is suppressed for potentials $\leqslant$300 mV in Ca^{2+} compared to Na^+ solutions. In

NaCl solution, the revival of the U^{V} signal and the accompanying decrease in U^{VI} at the most positive potentials was shown [40] to be due to the development of local acidity within cracks, sites of missing grains, and asperities in the fuel surface.

3.4. Anodic oxidations at 250 mV with varying $[Ca^{2+}]$ (96 h)

To determine the influence of Ca^{2+} on the development of local acidity, a series of anodic dissolution experiments were performed in solutions with different Ca^{2+} concentrations. A potential of 250 mV was chosen since the development of local acidity was observed in NaCl solutions at this potential and it is still in the potential range where the XPS results, Fig. 7, show Ca^{2+} suppresses the formation of surface U^{VI} species which has been claimed to be a prerequisite for acidification. The experiments were conducted over 96 h since 1 h is commonly too short a period of oxidation for the development of acidity to be observed.

Fig. 9 shows that the recovery in anodic current symptomatic of the development of localized acidity is severely suppressed, but not totally prevented, as the Na^{+} cation is replaced with Ca^{2+}. This is most clearly illustrated in Fig. 10 which shows the anodic charges for dissolution obtained by the integration of *I–t* curves in Fig. 9. A measure of the effectiveness of Ca^{2+} in suppressing the dissolution current is the percentage suppression ($\%_{sup}$)

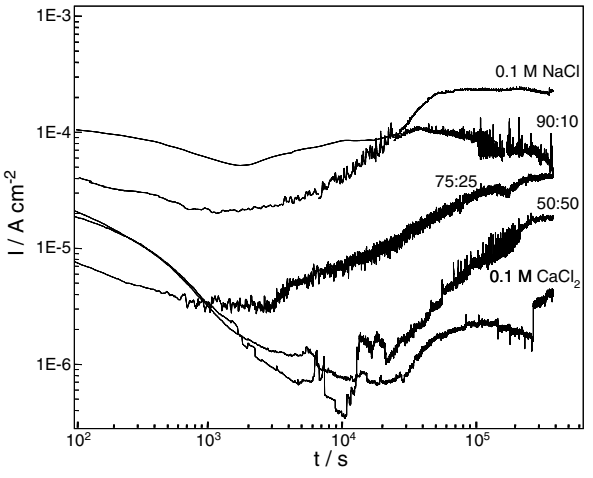

Fig. 9. Potentiostatic current–time curves recorded for 96 h at 250 mV in 0.1 mol L^{-1}solutions containing different ratios of $CaCl_2$ and NaCl at pH 9.5.

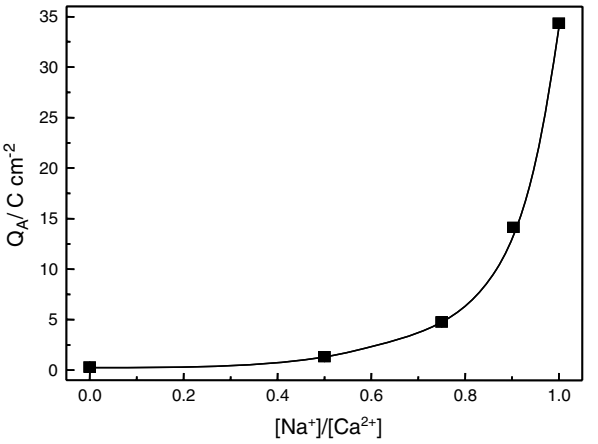

Fig. 10. Anodic charges for dissolution obtained by the integration of *I–t* curves from Fig. 9.

$$\%_{sup} = \frac{(Q_A)_0}{(Q_A)_0 + (Q_A)_1} \times 100, \quad (2)$$

where $(Q_A)_0$ is the charge without any Ca^{2+} in solution and $(Q_A)_1$ is the calculated charge in a 0.1 mol L^{-1} Ca^{2+} solution. This calculation shows that the complete replacement of Na^{+} by Ca^{2+} suppresses dissolution by 99.1%.

SEM micrographs were recorded after these 96 h anodic oxidations and are shown in Fig. 11(A)–(F). There is no discernible difference in the state of the surface after oxidation in 0.1 M $CaCl_2$, Fig. 11(B) compared to a freshly prepared specimen, Fig. 11(A). As the Ca^{2+} cation is progressively replaced by Na^{2+}, Fig. 11(C)–(F), there is an increase in the development of dissolved trenches and small pits, due to the enhancement of dissolution by local acidity and consistent with the increased current at long times and the overall increase in dissolution charge in a 0.1 mol L^{-1} NaCl solution, Fig. 9.

3.5. Effect of varying $[Ca^{2+}]$ in solutions

In an attempt to investigate the influence of Ca^{2+} in the absence of local acidification, a series of anodic oxidation experiments were performed at the lower applied potential of 100 mV in solutions with various $[Na^{+}]/[Ca^{2+}]$ ratios for 18 h, Fig. 12. At this potential the influence of this ratio on the initial stages of the transformation of $U^{IV}_{1-2x}U^{V}_{2x}O_{2+x}$ to U^{VI} species should be more readily apparent. In 0.1 mol L^{-1} $CaCl_2$ there is no indication of any increase in current at long times, Fig. 12 (i), indicative of the development of local acidity and the formation of soluble U^{VI} species. There is a

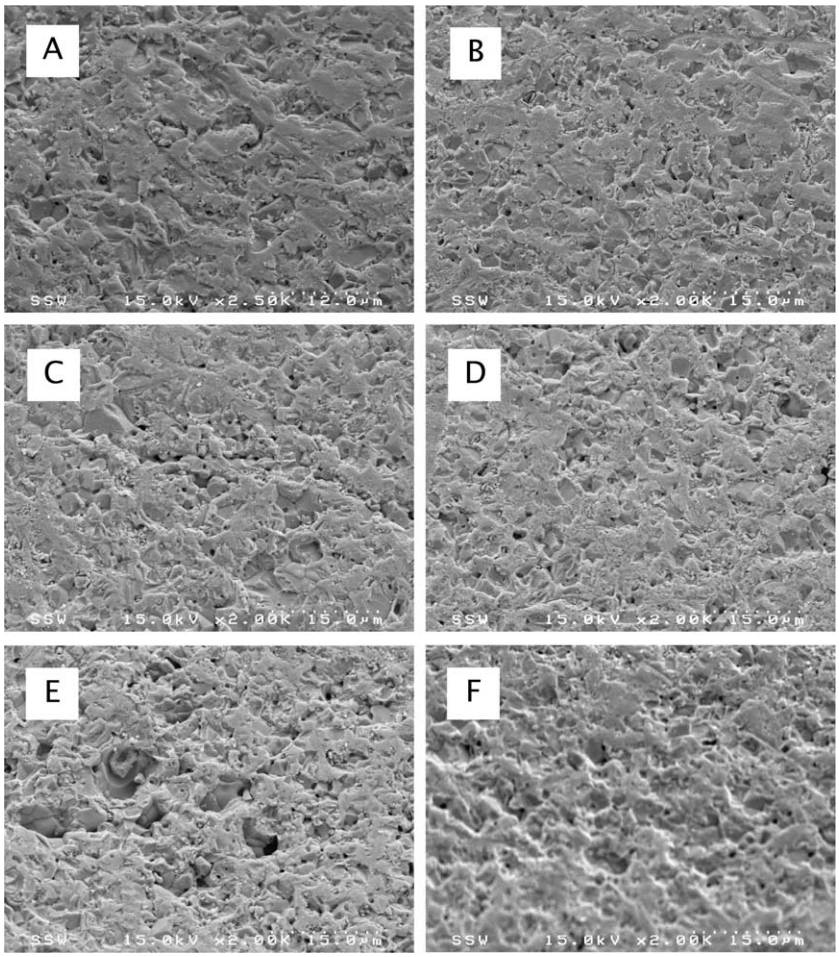

Fig. 11. SEM micrographs at a magnification of 2000X on a 1.5 at.% SIMFUEL electrode after (A) polishing to a 1200 grit surface, and after anodic oxidation for 96 h at 250 mV in various $[Ca^{2+}]$ (mol L^{-1}) solutions: (B) 0.1, (C) 0.05, (D) 0.025, (E) 0.01 and (F) 0 (0.1 mol L^{-1} NaCl).

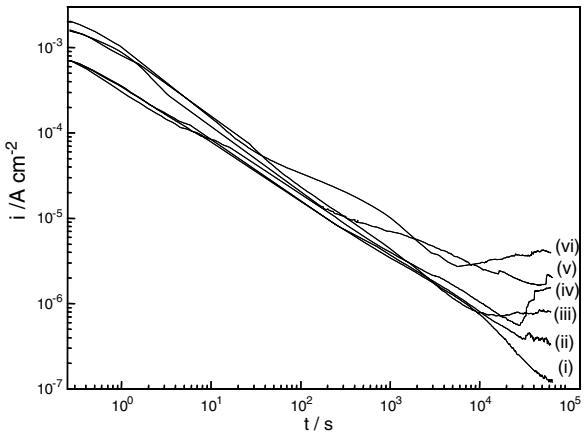

Fig. 12. Potentiostatic current–time curves recorded on 1.5 at.% SIMFUEL in 0.1 mol L^{-1}solutions (pH 9.5) with various $[Ca^{2+}]/[Na^{+}]$ ratios, at an applied potential of 100 mV for 18 h (i) 1, (ii) 0.8, (iii) 0.65, (iv) 0.5, (v) 0.25 and (vi) 0.

tendency towards the achievement of steady-state currents for $t > 10^4$ s as Ca^{2+} is gradually replaced with Na^{+}, Fig. 12 (ii)–(vi).

Fig. 13 shows the proportions of the three U oxidation states as a function of the fraction of $[Ca^{2+}]$ in solution. The high U^{V} content in the presence of Ca^{2+} confirms that its presence does not suppress the $UO_2 \rightarrow U^{IV}_{1-2x}U^{V}_{2x}O_{2+x}$ oxidation step. The relative amount of U^{VI} in the electrode surface increases once the fraction of Ca^{2+} drops below ~0.25, consistent with the loss of suppression by Ca^{2+} of the oxidative dissolution (as UO_2^{2+}) and subsequent deposition (as $UO_3 \cdot yH_2O$) process. The amount of Ca found on the surface of the electrode steadily increased from 0% (0.1 mol L^{-1} NaCl) to 11% in 0.1 mol L^{-1} $CaCl_2$, Fig. 14. While a signal for Cl^{-} was also observed in the XPS spectra, the amount

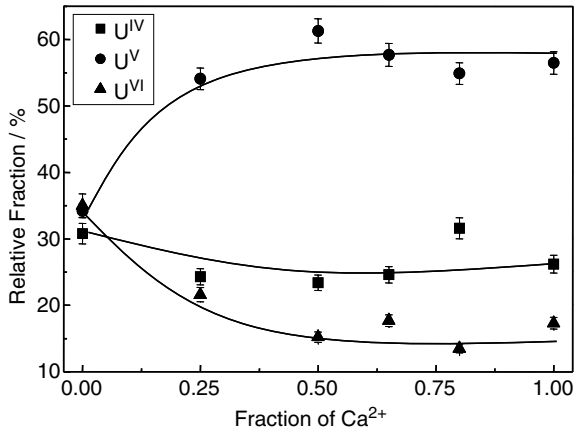

Fig. 13. Relative fractions of all three U oxidation states in the surface of 1.5 at.% SIMFUEL oxidized at 100 mV for 18 h as a function of the fraction of Ca^{2+} present in $NaCl/CaCl_2$ solutions with an overall concentration of 0.1 mol L^{-1}.

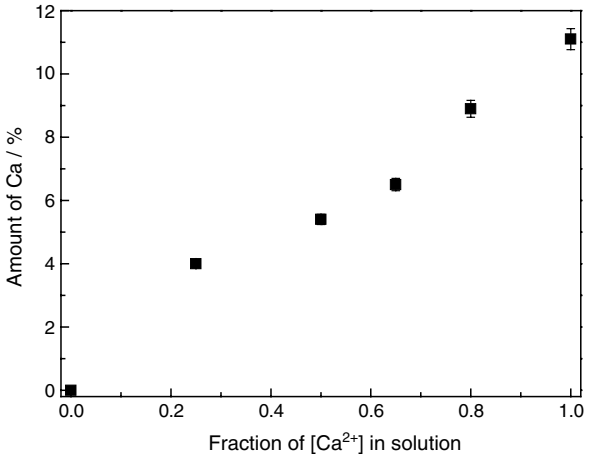

Fig. 14. Fraction of Ca^{2+} in the surface of 1.5 at.% SIMFUEL in $NaCl/CaCl_2$ solutions with an overall concentration of 0.1 mol L^{-1}.

of Cl^- on the electrode surface did not increase in proportion to the increase in Ca^{2+}, suggesting Ca^{2+} incorporation into the electrode surface was an integral feature of the suppression of the oxidation/dissolution process at 100 mV. This observation should be contrasted with our inability to find any consistent evidence for Ca^{2+} incorporation for more positive applied potentials (Section 3.3).

4. Discussion

Observations made electrochemically with the support of XPS suggest that Ca^{2+} does not influence the conversion of $U^{IV}O_2$ to $U^{IV}_{1-2x}U^{V}_{2x}O_{2+x}$. This is not surprising since the nature of the electrolyte cation would not be expected to influence the injection of O^{2-} ions into interstitial sites in the UO_2 fluorite lattice, a process accompanied by the oxidation of U^{IV} to U^{V} within the electrode surface. However, there is clear evidence for the influence of the cation on the conversion reaction

$$(U^{V})_{\text{lattice}} \rightarrow (U^{VI})_{\text{surface}} \rightarrow (UO_2^{2+})_{\text{solution}} \rightarrow (UO_3 \cdot yH_2O)_{\text{deposit}} \quad (3)$$

As discussed in the introduction, Ca^{2+} (and Na^+) is expected to incorporate into U^{VI} deposits on the fuel surface under oxidizing conditions. However, our results show that the accumulation of U^{VI} on the electrode surface under moderately oxidizing conditions (100 mV) decreases as the Ca^{2+} content of the surface increases; i.e., Ca^{2+} suppresses U^{VI} formation rather than stabilizing it in the form of a Ca^{2+}-containing deposit.

Previous results by Scott et al. [47] have shown that significant cation effects are observed for the chemical dissolution of β-$U^{VI}O_3$ in both acidic and carbonate solutions. In acidic solutions ($1 \leqslant pH \leqslant 3$) the ability of cations to suppress the dissolution rate was in the order; $Mg^{2+} \geqslant Li^+ > Na^+ > NH_4^+ > K^+ > Cs^+$ and in carbonate solutions; $Na^+ > NH_4^+ > Cs^+ \geqslant K^+$. These effects were explained according to the charge transfer theory of Engell [48] and Vermilyea [49] (summarized in Ref. [50]), in which the dissolution process is seen as the transfer of ions across the oxide/solution interface and rate-control can be due to either cation or anion transfer processes. According to this theory, cations can influence the dissolution rate by blocking the anion (O^{2-}) interfacial transfer sites. The transfer of oxide anions to solution involves their neutralization by protons

$$(O^{2-})_{\text{lattice}} + 2H^+ \rightarrow H_2O \quad (4)$$

and the displacement of protons by cations from surface anion sites would suppress the rate of this ion transfer step.

The ability of a cation to displace H^+ from these surface sites will be promoted by its polarizability (proportional to the cation charge/radius ratio) but hindered by its energy of hydration in aqueous solutions. The sequence of cation effects determined by Scott et al. [47] indicates that it is the hydration energy

that exerts the primary influence on cation adsorption; i.e., the more strongly hydrated the cation the more weakly it is adsorbed and the less influence it exerted on the oxide dissolution process.

These effects offer a basis for an interpretation of the influence of Ca^{2+} on the oxidative dissolution of UO_2. By comparison to the cation sequence determined by Scott et al. we would expect the doubly charged Ca^{2+} to be more strongly adsorbed on UO_2 surfaces than Na^+. Radii [51] and hydration energies [52] for Ca^{2+} and Na^+, suggest that the charge to radius ratio; $\left(\frac{Z}{r}\right)_{Ca^{2+}} > \left(\frac{Z}{r}\right)_{Na^+}$ is a stronger influence in displacing H^+ on the surface of UO_2 than the hydration enthalpies $(\Delta H_{hyd})_{Ca^{2+}} \ll (\Delta H_{hyd})_{Na^+}$.

The creation of a precursor U^{VI} dissolution site would be expected to involve the extraction of an oxidized U^V cation from the fuel matrix and its stabilization on the surface as a hydrolyzed species,

$$\begin{aligned}(U^V)_{lattice} &\rightarrow (U^{VI})_{lattice} + 4H_2O \\ &\rightarrow (UO_2(OH)_2)_{ads} + 4H^+ \end{aligned} \quad (5)$$

a process that must be accompanied by the neutralization of two O^{2-} ions by protons and then their transfer to aqueous solution via reaction (4).

There are then two means by which Ca^{2+} adsorption could suppress the formation of U^{VI} surface species as observed in our experiments;

(i) It could inhibit stabilization of the cation precursor to dissolution, $(UO_2(OH)_2)_{ads}$, by preventing its stabilization by OH^- incorporation.
(ii) It could block the anion transfer reaction via reaction (4) by displacing protons from the anion transfer sites, a process that would, therefore, inhibit the formation of the U^{VI} surface precursor to dissolution.

Subsequently, since the formation and release to solution of UO_2^{2+} is severely suppressed, the hydrolysis to produce acidity,

$$UO_2^{2+} + yH_2O \rightarrow UO_2(OH)_y^{(2-y)+} + 2yH^+ \quad (6)$$

would also be inhibited as observed in our experiments. Such a direct cation effect on the oxidative dissolution process would be expected to be rapidly established and would account for the immediate response of the dissolution rate of UO_2 and spent fuel to the addition of Ca^{2+} in single-pass flow-through experiments reviewed in the introduction.

5. Summary and conclusions

Anodic currents observed in potentiostatic experiments are consistently lower in Ca^{2+} as compared to Na^+ solutions. The higher U^V, and lower U^{VI}, contents of the surface observed with XPS suggest that Ca^{2+} does not influence the surface oxidation process (reaction (1)) but suppresses the subsequent formation of surface U^{VI} species which are thought to form via a dissolution (as UO_2^{2+})–deposition ($UO_3 \cdot yH_2O$) process (reaction sequence (3)).

SEM analyses illustrated that as the Ca^{2+} cation is progressively replaced by Na^+ there is an increase in the development of dissolved trenches and small pits, due to the enhancement of dissolution by local acidity. This is consistent with the increased anodic dissolution currents and the overall increase in dissolution charge in Na^+ compared to Ca^{2+} solutions. XPS suggests that Ca^{2+} incorporation into the electrode surface is an integral feature of the suppression of the oxidation/dissolution process.

There two possibilities by which Ca^{2+} adsorption could suppress the formation of U^{VI} surface species: adsorption of Ca^{2+} on the UO_2 surface could suppress fuel dissolution either via inhibiting the stabilization of the cation precursor to dissolution $(UO_2(OH)_2)_{ads}$ or by blocking the O^{2-} anion transfer reaction from the fuel surface. These results offer an explanation for the suppression of the intrinsic corrosion rate of UO_2 observed in single-pass flow-through experiments on addition of calcium ions.

Acknowledgements

This research was funded under the Industrial Research Chair agreement between the Canadian Natural Sciences and Engineering Research Council (NSERC) and Ontario Power Generation (OPG), Toronto. Surface Science Western supplied the SSX-100 used for XPS analyses.

References

[1] L.H. Johnson, D.W. Shoesmith, in: W. Lutze, R.C. Ewing (Eds.), Radioactive Waste Forms for the Future, Elsevier, Amsterdam, 1988, p. 635.
[2] L.H. Johnson, D.M. Le Neveu, F. King, D.W. Shoesmith, M. Kolar, D.W. Oscarson, S. Sunder, C. Onofrei, J.L. Crosthwaite, Atomic Energy of Canada Limited Report, AECL-11494-2, COG-95-552–2, 2000.
[3] S. Sunder, Atomic Energy of Canada Limited Report, AECL-11380, COG-95-340, 1995.

[4] D.W. Shoesmith, J. Nucl. Mater. 282 (2000) 1.
[5] D.W. Shoesmith, M. Kolar, F. King, Corrosion 59 (2003) 802.
[6] P.C. Burns, R.C. Ewing, M.L. Miller, J. Nucl. Mater. 245 (1997) 1.
[7] E.C. Buck, R.J. Finch, P.A. Finn, J.K. Bates, Mater. Res. Soc. Symp. Proc. 506 (1998) 83.
[8] R.J. Finch, J.A. Fortner, E.C. Buck, S.F. Wolf, Mater. Res. Soc. Symp. Proc. 713 (2002) 647.
[9] P.C. Burns, K.M. Deely, S. Skanthakumar, Radiochim. Acta 92 (2004) 151.
[10] E.C. Buck, D.J. Wronkiewicz, P.A. Finn, J.K. Bates, J. Nucl. Mater. 249 (1997) 70.
[11] D.J. Wronkiewicz, J.K. Bates, S.F. Wolf, E.C. Buck, J. Nucl. Mater. 238 (1996) 78.
[12] D.J. Wronkiewicz, J.K. Bates, T.J. Gerding, E. Veleckis, B.S. Tani, Nucl. Mater. 190 (1992) 107.
[13] R.J. Finch, E.C. Buck, P.A. Finn, J.K. Bates, in: D.J. Wronkiewicz, J.H. Lee (Eds.), Scientific Basis for Nuclear Waste Management XXII, Mater. Res. Soc. Symp. Proc., vol. 556, 1999, p. 431.
[14] Office of Civilian Radioactive Waste Management. CSNF Waste Form Degradation: Summary Abstraction ANL-EBS-MD-000015 REV 02, 2004.
[15] M.-P. Lahalle, R. Guillamont, G.C. Allen, J. Chem. Soc. Faraday Trans. 86 (1990) 2641.
[16] R.J. Finch, R.C. Ewing, Radiochim. Acta 52 (3) (1991) 395, Part 2.
[17] R.J. Finch, R.C. Ewing, J. Nucl. Mater. 190 (1992) 133.
[18] D.J. Wronkiewicz et al., in: Uranium: Mineralogy, Geochemistry and the Environment, Mineralogical Society of America, Washington, DC, 1999, p. 475.
[19] M. Amme, T. Wiss, H. Thiele, P. Boulet, H. Lang, J. Nucl. Mater. 341 (2005) 209.
[20] K.-A. Kubatko, K.B. Helean, A. Navrotstiy, P.C. Burns, Science 302 (2003) 1191.
[21] L.E. Eary, L.M. Cathles, Metall. Trans. B 14B (1983) 325.
[22] R.A. Brown, Soc. Min. Eng. AIME 270 (1980) 1836.
[23] B. McNamara, E. Buck, B. Hanson, Mater. Res. Soc. Symp. Proc. 757 (2003) 401.
[24] P. Diaz-Arocas, J. Quinones, C. Maffiotte, J. Serrano, J. Garcia, J.R. Almazan, J. Esteban, Mater. Res. Soc. Symp. Proc. 353 (1995) 641.
[25] R. Wang, Pacific Northwest Laboratories Report, Richland Washington, PNL-3566, 1981.
[26] F. Clarens, J. de Pablo, I. Diez-Perez, I. Casas, J. Gimenez, M. Rovira, Environ. Sci. Technol. 38 (2004) 6656.
[27] G. Sattonay, C. Ardois, C. Corbel, J.F. Luichini, M.-F. Barthe, F. Garrido, D. Gosset, J. Nucl. Mater. 288 (2001) 11.
[28] P.C. Burns, K.-A. Hughes, Am. Miner. 88 (2003) 1165.
[29] J. Eejka, J. Dejkora, M. Delinees, N. Jb. Miner. 3 (1996) 125.
[30] P.C. Burns, R.J. Finch, F.C. Hawthorne, M.L. Miller, R.C. Ewing, J. Nucl. Mater. 249 (1997) 199.
[31] C.N. Wilson, W.J. Gray, Mater. Res. Soc. Symp. Proc. 176 (1990) 489.
[32] J.C. Tait, J.M. Luht, Ontario Hydro Report No. 06819-REP-01200-0006-ROO, 1997.
[33] J.L.M. Luht, MSc thesis, University of Manitoba, Winnipeg, 1998.
[34] G.J. Hyland, J. Ralph, High Temp. High Press. 15 (1983) 179.
[35] N.J. Dudney, R.L. Coble, H.L. Tuller, J. Am. Ceram. Soc. 64 (1981) 627.
[36] P.W. Winter, J. Nucl. Mater. 161 (1989) 38.
[37] P.G. Lucuta, R.A. Verrall, H. Matzke, B.J.F. Palmer, J. Nucl. Mater. 178 (1991) 48.
[38] P.G. Lucuta, B.J.F. Palmer, H. Matzke, D.S. Hartwig, in: I.J. Hastings (Ed.), Proceedings of the 2nd International Conference on CANDU Fuel, 1989, p. 132.
[39] H. Matzke, P.G. Lucuta, R.A. Verrall, J. Nucl. Mater. 185 (1991) 292.
[40] B.G. Santos, H.W. Nesbitt, J.J. Noël, D.W. Shoesmith, Electrochim. Acta 49 (2004) 1863.
[41] D.A. Shirley, Phys. Rev. B 5 (12) (1972) 4709.
[42] S. Van den Berghe, J.P. Laval, B. Gaudreau, H. Terryn, M. Verwerft, J. Nucl. Mater. 277 (2000) 28.
[43] J.F. Moulder, W.F. Stickle, P.E. Sobol, K.D. Bomben, J. Chastain (Eds.), Handbook of X-ray Photoelectron Spectroscopy, Perkin-Elmer Corp., MN, USA, 1992.
[44] D.W. Shoesmith, S. Sunder, W.H. Hocking, in: J. Lipkowski, P.N. Ross (Eds.), Electrochemistry of Novel Materials, vol. 1, VCH, New York, 1994, p. 297.
[45] I. Grenthe, H. Wanner, I. Forest (Eds.), Chemical Thermodynamics of Uranium, NEA-OECD, Chemical Thermodynamics, vol. 1, North Holland, Amsterdam, 1992, p. 323.
[46] B.G. Santos, J.J. Noël, D.W. Shoesmith, J. Electroanal. Chem. 586 (2006) 1.
[47] P.D. Scott, D. Glasser, M.J. Nicol, J. Chem. Soc. Dalton (1977) 1939.
[48] H.-J. Engell, J. Phys. Chem. (Leipzig) 7 (1956) 158.
[49] D.A. Vermilyea, J. Electrochem. Soc. 113 (1966) 1067.
[50] R.L. Segall, R.S.C. Smart, P.S. Turner, in: Surface and Near-Surface Chemistry of Oxide Materials, Elsevier Science, Amsterdam, 1988, p. 527.
[51] G. Wulfsberg, Principles of Descriptive Chemistry, Cole Publishing, Monterey CA, 1987, p. 23.
[52] J. Burgess, Metal Ions in Solutions, Ellis Horwood, Chichester, England, 1978, p. 182.